ELSEVIER

Polymer 42 (2001) 2611–2619

polymer

www.elsevier.nl/locate/polymer

LCP droplet deformation in fiber spinning of self-reinforced composites

C.H. Song, A.I. Isayev*

Institute of Polymer Engineering, The University of Akron, Akron, OH 44325-0301, USA

Received 17 March 2000; received in revised form 23 June 2000; accepted 12 July 2000

Abstract

The development of morphology during fiber spinning of blends of polyesters (PET and PBT) with LCP (PET/HBA) was studied. The quantitative predictions of the blend morphologies under isothermal and non-isothermal conditions were obtained using a droplet deformation criteria based on the reduced capillary number and the affine deformation theory. The temperature, radius, velocity, and strain rate profiles of 60/40 polyester/LCP fibers along the spin line were calculated using Kase and Matsuo's theory for fiber spinning under the steady-state condition. Simulation of breakup of LCP phase during fiber spinning of the blend based on the dimensionless breakup time indicated the absence of their breakup. The flow curves of the blends at various temperatures required to carry out simulation were obtained by a capillary rheometer. An Arrhenius type equation was established for the viscosity variation with the temperature. An interfacial tension between the components was calculated from the interfacial thickness observed by SEM. In the calculation, various viscosity ratios between thermoplastics and LCP components were applied. Initial and final sizes of LCP phase were examined by SEM and image analyzer. The calculated diameters of LCP fibrils in the fibers were found to be in agreement with the measured values.

Keywords: Polyester/LCP blends; Fiber spinning; Droplet deformation criteria

1. Introduction

The morphology of immiscible polymer blends largely influences the mechanical or barrier properties of the blends. Therefore, the modeling and controlling of the morphology development during melt processing are important. However, the prediction of the final morphology is not clearly established due to the complexity of the temperature and flow field; the competition between deformation, breakup, and coalescence of the dispersed phase; and the viscoelastic nature of phases. A better understanding of the deformation phenomenon of droplets can lead to an optimization of blend's properties.

The fibrillation of the LCP phase in polyester matrices promotes the mechanical properties of the blends to a great extent (for review see Ref. [1]). Specifically, the properties of the blend depended on the degree of deformation, the size, and the shape of the LCP phase. These morphologies are primarily controlled by the melt processing conditions. Proper control of these conditions can lead to an optimization of the blend properties [2–4]. However, there has been no effort in the literature to establish a quantitative relationship between the processing conditions and morphologies in thermoplastic/LCP blends.

Taylor [5,6] performed the pioneering research on the deformation of a drop in a Newtonian fluid. Taylor [5] calculated the velocity and pressure fields inside and outside the droplet by solving Stoke's equation for creeping flow. Taylor [6] also obtained expressions for the deformability D of the droplet for low-strain conditions. The deformability D is expressed as:

$$D = \frac{(L - B)}{(L + B)} \tag{1}$$

where L is the length and B the breadth of the deformed ellipsoid. Taylor's results indicated that the droplet deformation and the shape of droplet depend on two dimensionless parameters, the capillary (Weber) number, Ca, and the viscosity ratio, p. The capillary number is the ratio of the hydrodynamic stress to the interfacial stress σ/R. In the case of the steady shear flow of Newtonian phases, the capillary number is expressed as:

$$\mathrm{Ca} = \frac{\text{hydrodynamic stress}}{\text{interfacial stress}} = \frac{\eta_m \dot{\gamma} R}{\sigma} \tag{2}$$

where η_m is the matrix viscosity, $\dot{\gamma}$ the shear rate, R the drop radius, and σ the interfacial tension. The viscosity ratio, p, is

* Corresponding author. Tel.: +1-330-972-6865; fax: +1-330-258-2339.
E-mail address: aisayev@uakron.edu (A.I. Isayev).

0032-3861/01/$ - see front matter
PII: S0032-3861(00)00555-3

the ratio of the viscosities of the two phases expressed as:

$$p = \frac{\eta_d}{\eta_m} \tag{3}$$

where η_d is the viscosity of the dispersed phase.

When the interfacial tension effect dominates the viscous effect, i.e. $Ca \ll 1$, the deformation D and the orientation angle α of the droplet are expressed as;

$$D = Ca\left(\frac{19p + 16}{16p + 16}\right), \qquad \alpha = \frac{\pi}{4}. \tag{4}$$

Over the entire range of p from zero to infinity, the quantity $(19p + 16)/(16p + 16)$ in Eq. (4) varies from 1.0 to 1.187; therefore, D is nearly equal to Ca.

For the case where the interfacial tension forces are equal to viscous forces, i.e. $Ca = 1$, $p \gg 1$ [6],

$$D = \frac{5}{4}p, \qquad \alpha = \frac{\pi}{2} \tag{5}$$

Taylor observed that the experimental results of droplet deformation agreed with his theory at low rates of deformation in both uniform shear and plane hyperbolic flow. However, Taylor's theory is not applicable to the case in which the interfacial tension effect and the viscous effect are comparable.

Cox [7] extended Taylor's analysis and developed a first-order theory for the deformation of a droplet with a full range of viscosity ratios in the general time-dependent shearing flow field. For the steady shear flow, the droplet deformation is represented as:

$$D = \frac{5(19p + 16)}{4(p + 1)\sqrt{\left(\frac{20}{Ca}\right)^2 + (19p)^2}}$$

$$\alpha = \frac{\pi}{4} + 0.5\tan^{-1}\left(\frac{19pCa}{20}\right). \tag{6}$$

The capillary number has a critical value beyond which the droplet can no longer sustain further deformation, and it breaks up into a number of smaller droplets. Taylor [5] found that for $p = 1$, the shape of a droplet in steady shear flow becomes unstable for a critical capillary number, Ca_c, of the order of unity. The value of Ca_c depends strongly on the viscosity ratio p and the type of flow (simple shear or extension). The empirical relationships are expressed by Utracki and Shi [8].

For values of the capillary number below Ca_c, the drop usually reaches a steady and only slightly deformed equilibrium shape in which the deformation is determined by the order of Ca. If Ca is slightly higher than Ca_c, the breakup into smaller droplets can be expected due to a growing disturbance at the interface. If $Ca \gg Ca_c$, the interfacial stress becomes negligibly small compared to the hydrodynamic stress, and it is usually assured that the drop will deform affinely with the applied macroscopic deformation [9].

Chin and Han [10] and Van der Reijden-Stolk and Sara [11] computed the flow field in a conical channel for Newtonian fluids using the Cox theory [7] for time-dependent flows. The viscoelastic droplets or matrices are considered by Chin and Han [10], Elmendorp and Maalcke [12], and Milliken and Leal [13].

The analysis of Taylor and Cox is restricted to the case of small deformations. For large deformations, slender body mechanics were used to develop a mathematical analysis [14] with small capillary numbers and small viscosity ratios. In polymer blend processing, the cases of low viscosity ratios and large capillary numbers which develop the fibrillation of the domain are encountered.

According to Huneault et al. [15], drop deformation and breakup depend on the reduced capillary number, Ca^*, which is following:

$$Ca^* = \frac{Ca}{Ca_c} \tag{7}$$

Depending upon the value of Ca^* in both shear and elongation, the droplets will be either deformed or broken according to following criteria:

1. If $Ca^* < 0.1$, droplets do not deform.
2. If $0.1 < Ca^* < 1$, droplets deform without breakup.
3. If $1 < Ca^* < 4$, droplets deform, but they break conditionally.
4. If $Ca^* > 4$, droplets deform affinely with the rest of the matrix and extend into long stable filaments.

In the present study, the development of a polyester/LCP blend morphology in fiber spinning was studied. The quantitative predictions of the LCP phase dimensions under isothermal and non-isothermal conditions were performed based on the above criteria. The results were compared with the experimental data.

2. Experimental

Two polyesters were used as matrices: PET (Eastapak PET Polyester 7352/Eastman Chemical Company) with I.V. of 0.74 and T_m of 253°C and PBT (Ultradur KR 4036-Q692/BASF AG) with I.V. of 1.24 and T_m of 225°C. The thermotropic LCP used as a reinforcing phase was 18/82 PET/HBA copolyester (Rodrun LC-5000/Unitika Ltd) with a random chain structure and T_m of 278°C.

The materials were dried in a vacuum oven at 120°C for 24 h. Then they were physically mixed to make 60/40 polyester/LCP composition by weight. Melt blending was performed using a one inch single screw extruder (Killion Inc.) followed by a static mixer (Koch) at the melt temperature of 285°C in the screw zones. The die diameter was 10 mm. The extrudate from the die was cooled in a water bath located about 1.0 cm from the die and drawn by a take-up device at various speeds. The extension ratio was calculated as a ratio of die area to fiber cross-sectional area.

Table 1
Parameters used in melt spinning simulation

Data	Value		Unit
	60/40 PET/LCP	60/40 PBT/LCP	
Air temperature, T_a	25	25	°C
Glass transition temperature, T_g	78	55	°C
Die temperature, T_d	240	270	°C
Specific heat, C_P	1965	1350	J/Kg K
Initial spin line tension, F_i	1.0×10^{-1}	1.0×10^{-1}	N
Density, ρ	1400	1389	Kg/m^3
Melt flow rate, W	0.400×10^{-3}	0.887×10^{-3}	Kg/s
Interfacial tension between polyester and LCP, σ	0.175×10^{-3}	0.0597×10^{-3}	N/m
Die diameter, d	0.01	0.01	m
Heat conductivity of air at 25°C, k_F	26.14×10^{-3}	26.14×10^{-3}	W/m.K
Kinematic viscosity of air at 25°C, ν_F	15.71×10^{-6}	15.71×10^{-6}	m^2/s
Initial LCP droplet diameter, D_0	3.96×10^{-6}	13.52×10^{-6}	m
Viscosity ratio, p	0.01–100	0.01–100	–
Correction factor, $(1+K)$	100.5	100.5	–

An Instron Capillary Rheometer (model 3211) was used to measure the viscosity vs. shear rate for polyesters, LCP, and 60/40 polyester/LCP blends at three temperatures. Three capillary dies (1.0668 mm in diameter; L/D ratios of 15.7, 30, 44.5) were used. The diameter of the barrel was 9.525 mm. Five plunger speeds (2.54, 7.62, 25.4, 76.2, 254.0 mm/min) were applied. The Bagley end correction was applied for the calculation viscosities.

Morphology of the fractured surface of the polyester/LCP fibers were observed using SEM (Hitachi S-2150). A coating device was used to coat the fractured surface with a gold–palladium alloy. An image analyzer (Leica Q500MC) was used to calculate the average droplet dimensions.

3. Results and discussion

3.1. Numerical simulation of melt spinning

For fiber spinning under the steady-state condition, Kase and Matsuo [16] established the temperature and radius profiles of fibers in the spin line as the following:

$$\frac{dT}{dz} = -\frac{2\sqrt{\pi A}h(T-T_a)}{WC_P} \tag{8}$$

and

$$\frac{dA}{dz} = -\frac{F\rho}{W\eta_E}A \tag{9}$$

where T is the filament temperature, T_a the air temperature, z the spin line distance from the spinneret, A the filament cross sectional area, h the heat transfer coefficient, W the melt throughput, C_P is the specific heat, F the spin line tension, ρ the density, and η_E the elongational viscosity.

The heat transfer coefficient, h, is calculated from the Nusselt–Reynolds (Nu–Re) relation for air flowing parallel to a cylinder, which is approximated by:

$$Nu = 0.42Re^{0.334} \tag{10}$$

Reynolds number, Re, is defined as:

$$Re = \frac{2\upsilon R}{\nu_F} \tag{11}$$

and Nusselt number, Nu, as:

$$Nu = \frac{2hR}{k_F} \tag{12}$$

where υ is the filament velocity, R the radius of the filament, ν_F the kinematic viscosity of ambient air, and k_F the heat conductivity of ambient air. Substituting the definitions of Nu and Re in Eq. (10) and multiplying the right-hand side of the same equation by the correction factor $(1+K)$, h is described as:

$$h = 0.21k_F\sqrt{\frac{\pi}{A}}\left(\frac{2W}{\sqrt{\pi A}\rho\nu_F}\right)^{0.334}(1+K) \tag{13}$$

Here, the correction factor, $(1+K)$, is introduced to take into account the effect of transverse air velocity on heat transfer. The cooling rate of the spin line is determined by the correction factor. In calculation, the correction factor, $(1+K)$, is adjusted to match the distance between the die and water bath.

The Eqs. (8) and (9) are ordinary differential equations of the first order and they are solved numerically by the Runge–Kutta method [17]. These equations are an initial value problem. Initial temperature, T_0, and radius, R_0, are known, but the initial value of the spin line tension, F_0, is not known. The Newton–Raphson iterative method is used with an initially guessed value of F_0 The calculation is continued until the calculated radius of fibers closely approximates the radius calculated from the melt throughput and draw down ratio. The value of the initial spin line tension is adjusted until those radii are matched.

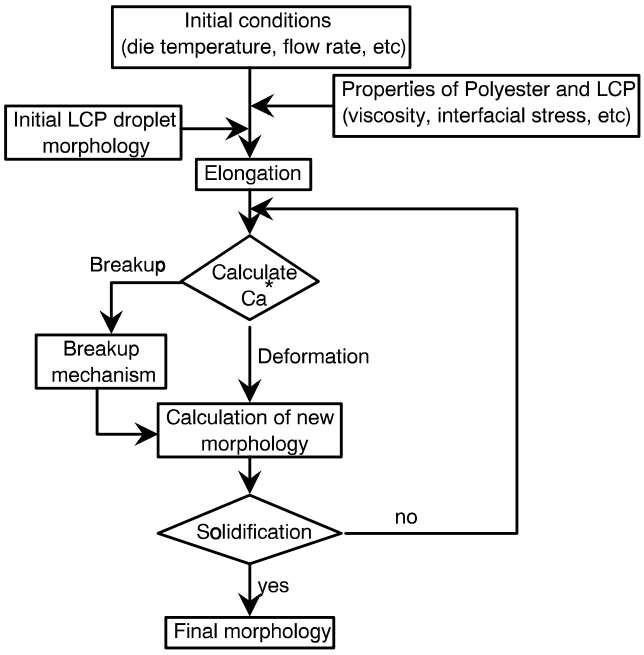

Fig. 1. The algorithm for calculation of LCP droplet deformation under uniaxial elongational flow.

The numerical solution is obtained at each point of the axial increment interval, Δz, to get the temperature and radius along the spin line. Once the filament radius profile is obtained, the velocity profile at each point on the spin line can be calculated from the mass conversion equation, $W = \rho V_z A_z$. Strain rate is calculated as:

$$\epsilon_z' = \frac{V_{z+1} - V_z}{\Delta z} = \frac{dV_z}{dz}. \quad (14)$$

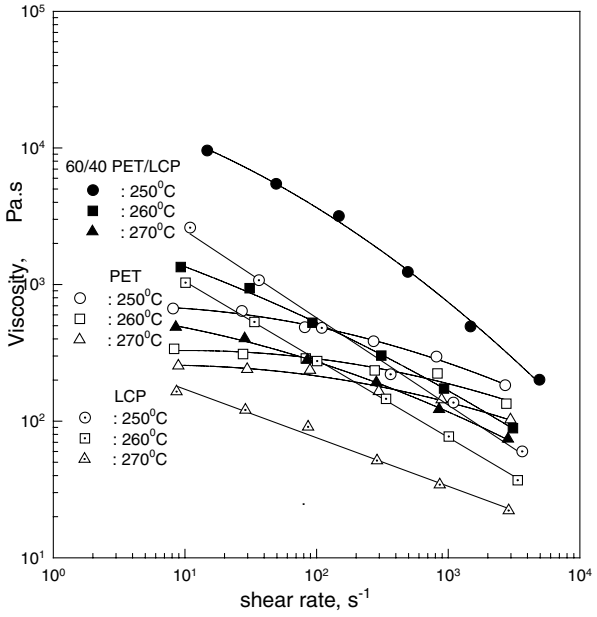

Fig. 2. Viscosity vs. shear rate curves for PET, LCP, and 60/40 PET/LCP at three different temperatures.

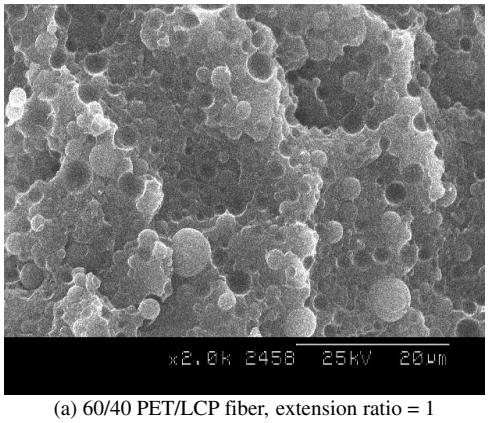

(a) 60/40 PET/LCP fiber, extension ratio = 1

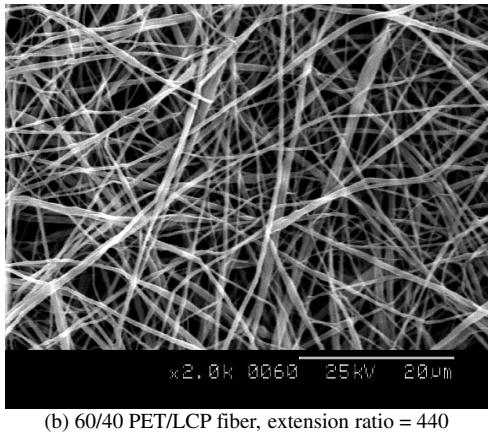

(b) 60/40 PET/LCP fiber, extension ratio = 440

Fig. 3. SEM photomicrographs of 60/40 PET/LCP fiber before (a) and after (b) elongation.

Parameters used in melt spinning simulation are given in Table 1.

3.2. Numerical simulation of LCP droplet deformation

The LCP droplet deformation in a polyester matrix under the melt spinning process is simulated based on Taylor's [5,6] theory in which Newtonian fluid was considered. The initial size of the LCP droplet at the die exit required for the calculation of droplet deformation is determined from SEM and the image analysis.

The deformation of a droplet depends on the reduced capillary number, Ca^* (Eq. (7)). The capillary number, which depends on strain rate, elongational viscosity, and droplet size, is calculated at each time step. The critical capillary number, Ca_c, depends on the viscosity ratio, p. In the elongational flow, Ca_c is calculated from the Grace's empirical equation [18]:

$$\log\left(\frac{Ca_c}{2}\right) = -0.64853 - 0.02442(\log p) + 0.02221(\log p)^2 - \frac{0.00056}{(\log p - 0.00645)} \quad (15)$$

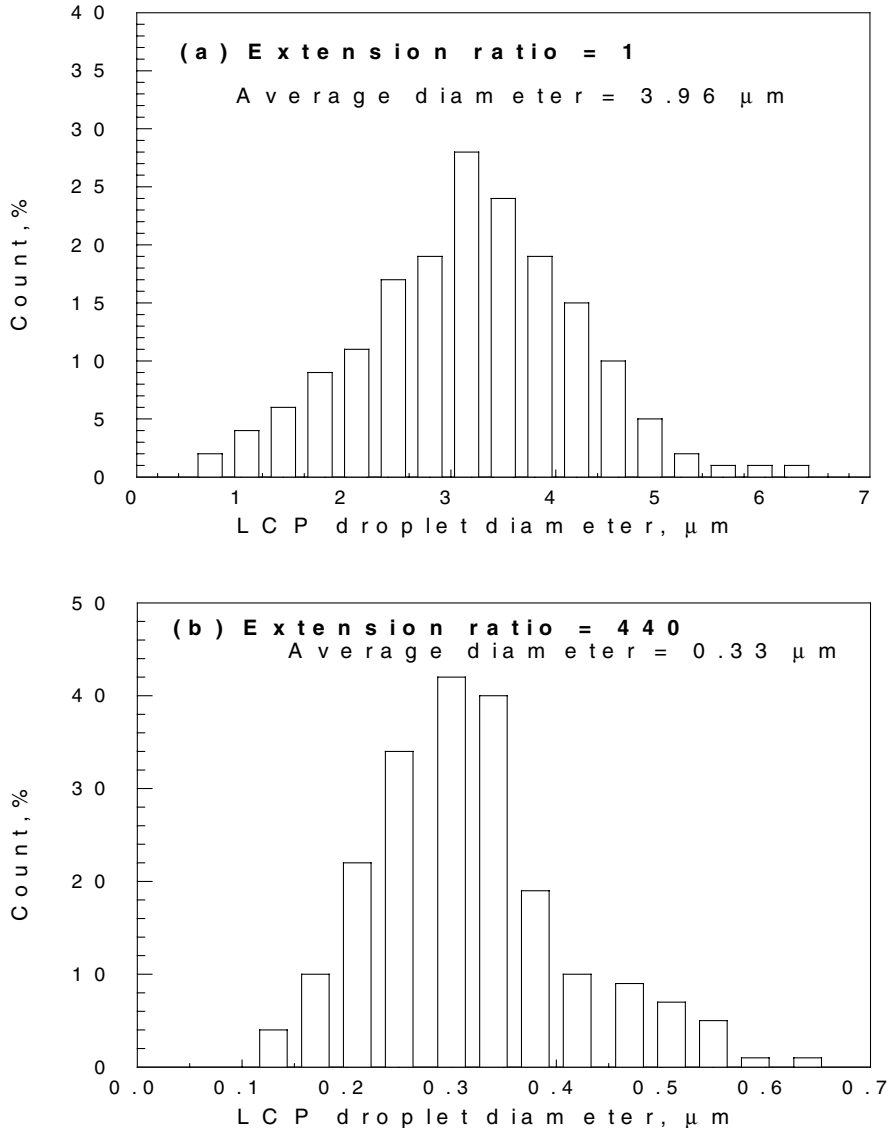

Fig. 4. Diameter of LCP phase in the fiber spinning of 60/40 PET/LCP at the extension ratios of 1 (a) and 440 (b).

The value of Ca is compared with Ca_c to determine if the deformation or breakup occurs [15].

For Ca^* between 0.1 and 4.0, the deformation is calculated by the linear deformation equation as suggested by Taylor (Eq. (4)). In the region $1.0 < Ca^* < 4.0$, the kinetics of the breakup depend on the viscosity ratio. The dimensionless breakup time is calculated as [8]:

$$t_b^* = \frac{t_b \gamma'}{Ca} = 84p^{0.345}\left(\frac{Ca}{Ca_c}\right)^{-0.559} \quad (16)$$

where t_b is the time for breakup and γ' the strain rate. Breakup does not occur if there is not enough time provided for the breakup before solidification.

As indicated by Huneault et al. [15], for $Ca^* > 4$, affine deformation occurs and the deformation is calculated by the exponential function for uniaxial deformation. For $Ca^* < 0.1$, no droplet deformation takes place. Therefore, calculations of droplet deformation were not performed.

The calculation of the deformation is continued until either the LCP fibrils' breakup or solidification occurs. If breakup occurs according to Utracki and Shi's breakup criterion (Eq. (16)) [8], then a new morphology is calculated. The calculation is terminated at solidification and the final dimensions of the LCP fibrils is plotted as a function of spin line distance. From this procedure, the sizes of the LCP droplets under different processing conditions in fiber spinning can be obtained.

The simulation is performed based on the following assumptions.

1. No coalescence of LCP droplets and no slip at the boundary occurs.

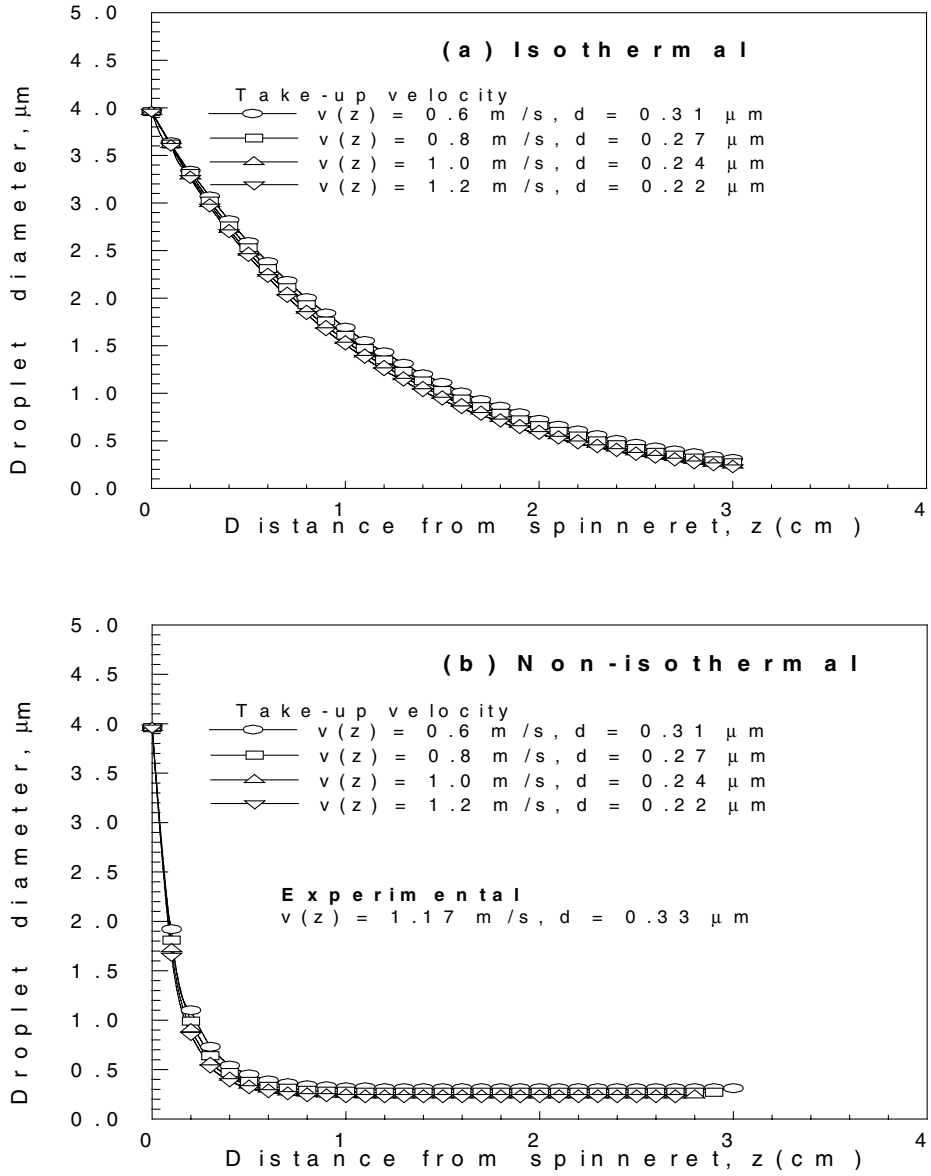

Fig. 5. Variation of LCP phase diameter along the spin line in the fiber spinning of 60/40 PET/LCP in isothermal (a) and non-isothermal (b) simulation.

2. Shear-induced orientation and crystallization are negligible.
3. Radial temperature profile in melt spinning is negligible.
4. If breakup occurs, new spherical droplets of equal diameter are generated.

The algorithm of the simulation is shown in Fig. 1.

3.3. 60/40 PET/LCP fiber

The viscosity of the PET, LCP, and 60/40 PET/LCP is shown in Fig. 2. The zero shear viscosity of the blend was calculated from the extrapolation of the flow curves at 250, 260, and 270°C. The temperature dependence of the zero shear viscosities, η_0, was obtained as:

$$\eta_0 = 1.5810 \times 10^{-31} \mathrm{e}^{\frac{42047.4}{T}} \tag{17}$$

The elongational viscosity, η_E, was calculated as

$$\eta_E = 3\eta_0 \tag{18}$$

As shown in Fig. 2, the viscosities of the 60/40 PET/LCP blend at 250, 260, and 270°C showed higher values than those of the LCP in the whole range of shear rates and PET at shear rates lower than 100 s^{-1}. The latter would indicate that the slip does occur in this blend. This high viscosity is also due to the high melting temperature of the LCP (278°C). Under the melting point of the LCP, the LCP particles behave like a filler which increases the viscosity of blends.

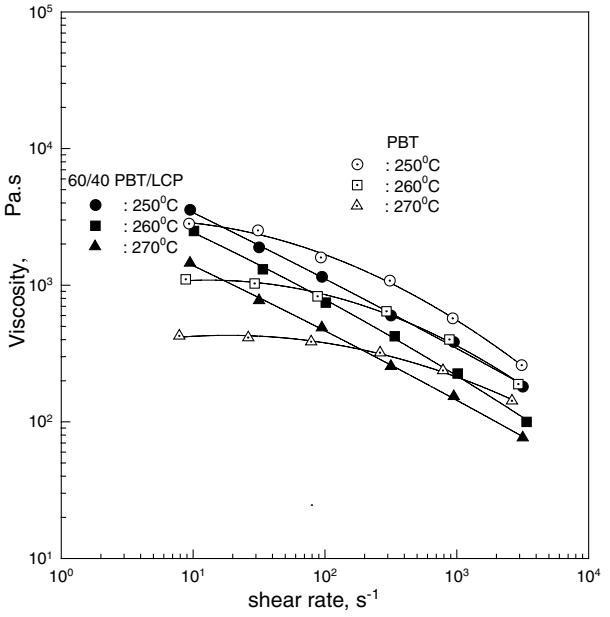

Fig. 6. Viscosity vs. shear rate curves for pure PBT and 60/40 PBT/LCP at three different temperatures.

SEM photomicrographs of the 60/40 PET/LCP fiber before and after elongation are shown in Fig. 3. Without extension, the LCP domains are spherical droplets. However, they deformed into long fibrils with an extension ratio of 440 as clearly seen after solvent extraction. The PET matrix was dissolved in boiling phenol for 24 h and the phenol was washed out by methanol. As seen from Fig. 3b, orientation of the LCP fibrils are somewhat distorted. There are two reasons for this to occur. During solvent extraction, stirring was applied to get a faster dissolution of the matrix leading to the distortion. Also, a possibility exists that some distortion took place during the transformation of the sample onto microscope slide after extraction. The distributions of LCP droplet diameters before and after elongation are shown in Fig. 4. The average diameter of the LCP droplets without extension was 3.96 μm. With an extension ratio of 440, the average diameter of the LCP fibrils was 0.33 μm.

The interfacial tension between PET and LCP was calculated from interfacial thickness according to Wu's relation [19]:

$$\gamma_{12} = 55 a_{\mathrm{I}}^{-0.86} \tag{19}$$

where the interfacial tension, γ_{12}, is in dyne/cm and the interfacial thickness, a_{I}, is in Å. The interfacial thickness observed by SEM was 800 Å leading to $\gamma_{12} = 0.175 \times 10^{-3}$ N/m.

Fig. 5 shows the variation in the calculated LCP phase diameter along the spin line. The monotonic decrease was observed under the isothermal spinning, while a fast decrease was observed at the spin line distance range from 0 to 0.5 cm under the non-isothermal spinning. This fast

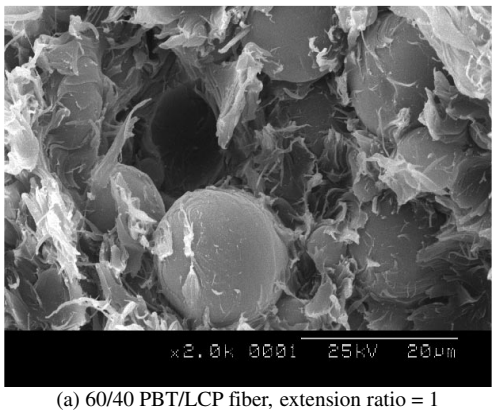

(a) 60/40 PBT/LCP fiber, extension ratio = 1

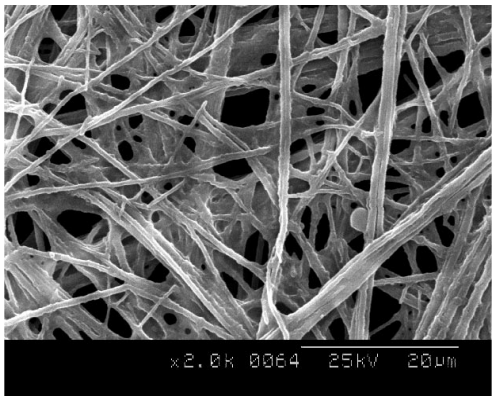

(b) 60/40 PBT/LCP fiber, extension ratio = 204

Fig. 7. SEM photomicrographs of 60/40 PBT/LCP fiber before (a) and after (b) elongation.

decrease in the LCP phase diameter along the spin line is due to a fast increase in the viscosity during cooling under the non-isothermal spinning. In both the isothermal and non-isothermal spinnings, the final LCP fibril diameter was 0.22 μm at a take-up velocity of 1.2 m/s. This value was close to the experimental diameter of 0.33 μm.

In both isothermal and non-isothermal cases, the LCP droplet was assumed to have a cylindrical shape and the deformation was calculated based on Utracki's criterion [15] with conservation of volume. In all cases, the reduced capillary number, Ca^{*}, was larger than 4.0. Therefore, the diameter, d, and length, L, of the LCP fibril after the deformation was based on affine deformation theory:

$$d = d_0 \exp\left(-\frac{\epsilon}{2}\right) \tag{20}$$

$$L = L_0 \exp(\epsilon) \tag{21}$$

where d_0 and L_0 are the original droplet diameter and length and ϵ the strain, which is calculated from the change of fiber diameter. Various viscosity ratios between LCP and PET components (0.01–100) were applied in the simulation, but no influence of the viscosity ratio on the LCP droplet deformation was found. It is evident that the LCP droplet deformation in PET matrix does not follow Taylor's

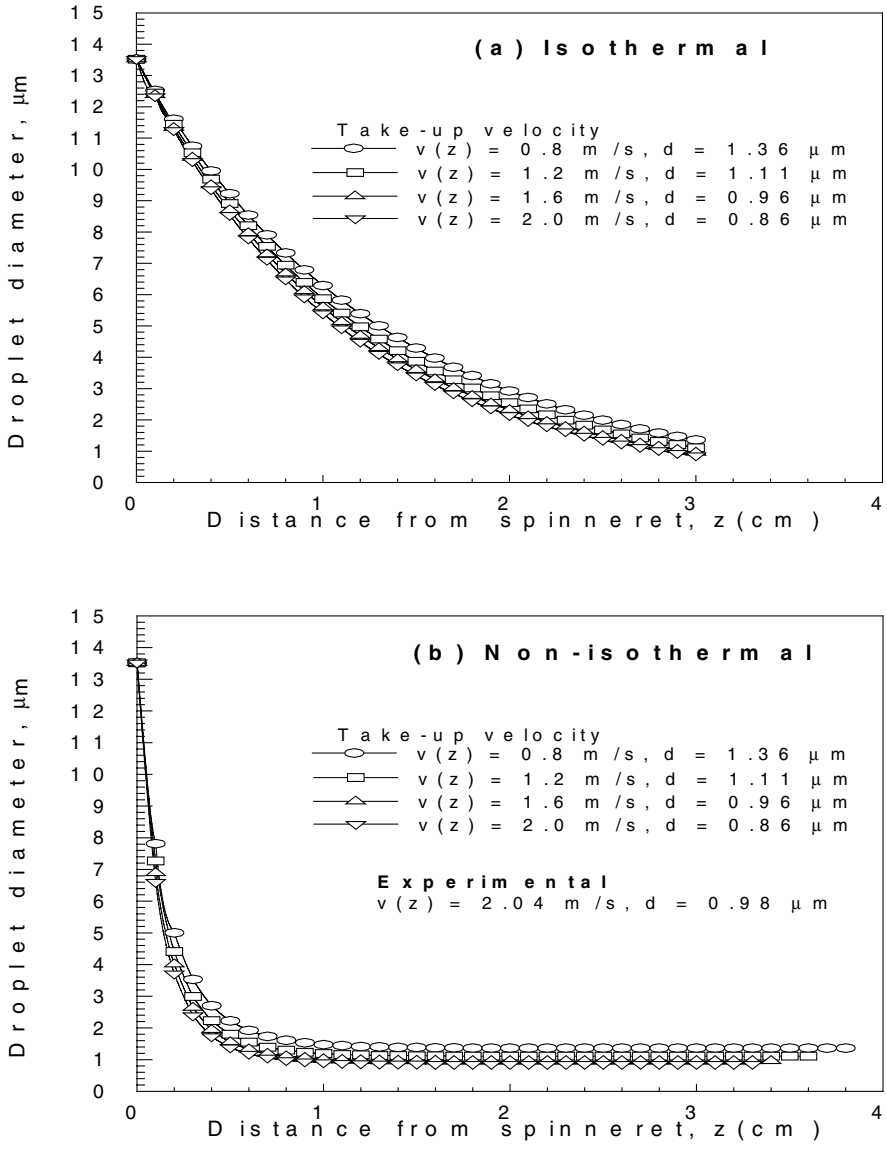

Fig. 8. Variation of LCP phase diameter along the spin line in the fiber spinning of 60/40, PBT/LCP in isothermal (a) and non-isothermal (b) simulation.

deformation theory, but follows the affine deformation theory. In simulation, no LCP breakup was observed. The final length of the LCP fibril was 1306 μm at a take-up velocity of 1.2 m/s in both the isothermal and non-isothermal calculations. It was not possible to measure the actual length of the fibrils because their ends were not found in the SEM photomicrographs. The maximum calculated aspect ratio of about 6000 was obtained at a take-up velocity of 1.2 m/s.

3.4. 60/40 PBT/LCP fiber

Fig. 6 shows the flow curves of the 60/40 PBT/LCP and the neat PBT. Similar to LCP (Fig. 2), the blend of 60/40 PBT/LCP (Fig. 6) showed almost power-law behavior. A smaller variation of viscosity with temperature variation was observed in the 60/40 PBT/LCP blend than in the neat PBT. This result is contrary to the PET case. In the blending of PBT/LCP, a partial miscibility was inferred by some researchers [20–24]. This partial miscibility might be a reason for the power-law behavior of viscosity and its lower variation with temperature. The obtained temperature dependence of zero shear viscosity is

$$\eta_0 = 1.1077 \times 10^{-7}\, \mathrm{e}^{\frac{13186.9}{T}} \tag{22}$$

A zero shear viscosity was taken at the shear rate of 6.5 s^{-1}.

Fig. 7 shows the shapes of the LCP domains in the PBT matrix before and after extension. The PBT matrix was extracted by 1/3 trifluoroacetic acid/methylene chloride solvent. The initial size of the spherical LCP droplets was much larger than that in the 60/40 PET/LCP blend. With an extension ratio of 204, the LCP fibrils were formed. The average diameter of the initial LCP droplets in the PBT

matrix was 13.52 μm, and it was reduced to 0.98 μm after the elongation.

The interfacial thickness was 2800 Å. From Wu's relation [19], the calculated interfacial tension was 0.0597×10^{-3} N/m. It is a lower value than that of the PET/LCP blend. Therefore, it can be inferred that due to the partial miscibility the better adhesion exists in the PBT/LCP blend than in the PET/LCP blend.

The variation of the calculated LCP domains along the spin line under the isothermal and non-isothermal conditions is shown in Fig. 8. In the non-isothermal spinning, the diameter decrease was largest at the distance range from 0 to 0.5 cm, and stabilized after 0.6 cm. With the take-up velocity of 2.0 m/s, the diameter of the LCP fibrils was 0.86 μm, and it was well matched to the experimental value of 0.98 μm.

The maximum calculated fibril length of 3300 μm was obtained with the take-up velocity of 2.0 m/s. In the computer simulation of the 60/40 PBT/LCP, no break up of LCP fibrils was observed, and the deformation of the LCP domain was performed based on the affine deformation theory, which is shown in Eqs. (20) and (21). The maximum aspect ratio of 3900 was obtained with a take-up velocity of 2.0 m/s. In the PBT/LCP blend, a lower aspect ratio of the LCP fibrils was obtained than in the PET/LCP blend. The partial miscibility between the components hinders the fibrillation. The partial miscibility led to less viscosity change with temperature. Therefore, a smaller strain was applied in the simulation leading to a lower aspect ratio of the LCP fibrils.

4. Conclusions

In the polyester/LCP blends, the LCP droplet deformation was calculated based on Utracki's criterion. At all take-up speeds, no breakup of the LCP phase appeared and the calculation was carried out by the affine deformation theory. The calculated LCP fibril diameter was well matched to the observation by SEM and the image analyzer. Because of the low viscosity of the LCP, favorable conditions for deformation in the PET matrix in a molten state are obtained. Therefore, Taylor's deformation theory, which considers the small deformation, was not applicable for LCP deformation. Instead, the affine deformation theory revealed a well-matched LCP deformation in the PET matrix. A lower aspect ratio of LCP fibrils in the 60/40 PBT/LCP fiber was obtained as compared to that in the 60/40 PET/LCP fiber. This was caused by the partial miscibility between the PBT and the LCP phase.

Acknowledgements

The authors wish to thank Unitika Ltd (LCP) and BASF AG (PBT) for their generosity in providing materials.

References

[1] Isayev AI. Liquid-crystalline polymer systems: technological advances. In: Isayev AI, Kyu I, Cheng SZD, editors. ACS symposium series, 632. Washington, DC: ACS, 1996. p. 1.
[2] Song CH, Isayev AI. SPE ANTEC 1998;44:1637.
[3] Song CH, Isayev AI. J Polym Engng 1998;18:417.
[4] Song CH, Isayev AI. SPE ANTEC 1999;45:2840.
[5] Taylor GI. Proc R Soc London 1932;A138:41.
[6] Taylor GI. Proc R Soc London 1934;A146:501.
[7] Cox RG. J Fluid Mech 1969;37:601.
[8] Utracki LA, Shi ZH. Polym Engng Sci 1992;32:1824.
[9] Meijer HEH, Jansen JMH. In: Manas-Zloczower I, Tadmor Z, editors. Mixing and compounding — theory and practical progress. Munich: Hanser, 1994.
[10] Chin HB, Han CD. J Rheol 1979;23:557.
[11] Van der Reijden-Stolk C, Sara A. Polym Engng Sci 1986;26:1229.
[12] Elmendorp JJ, Maalcke RJ. Polym Engng Sci 1985;25:1041.
[13] Milliken WJ, Leal LG. J Non-Newtonian Fluid Mech 1991;40:355.
[14] Taylor GI. Proceedings of 11th International Congress on Applied Mechanics, Munich, 790. Berlin: Springer, 1964.
[15] Huneault MA, Shi ZH, Utracki LA. Polym Engng Sci 1995;35:115.
[16] Kase S, Matsuo T. J Polym Sci A 1965;3:2541.
[17] Press WH. Numerical recipes in fortran. New York: Cambridge University Press, 1992.
[18] Grace HP. Chem Engng Commun 1982;14:225.
[19] Wu S. Polymer interface and adhesion. New York: Marcel Dekker, 1982 (p. 121).
[20] Kimura M, Porter RS. J Polym Sci, Polym Phys Ed 1984;22:1967.
[21] Ajji A, Gignac PA. Polym Engng Sci 1992;32:903.
[22] Pracella M, Chiellini E, Galli G, Dainelli D. Mol Cryst Liq Cryst 1987;153:525.
[23] Pracella M, Dainelli D, Galli G, Chiellini E. Makromol Chem 1986;187:2387.
[24] Paci M, Barone C, Magagnini P. J Polym Sci, Polym Phys 1987;25:1595.